Original article

Antibacterial activity of biosynthesized gold nanoparticles using biomolecules from *Lignosus rhinocerotis* and chitosan

Haliza Katas [a,*], Chei Sin Lim [a], Ahmad Yasser Hamdi Nor Azlan [a], Fhataheya Buang [a], Mohd Fauzi Mh Busra [b]

[a] *Centre for Drug Delivery Research, Faculty of Pharmacy, Universiti Kebangsaan Malaysia, Jalan Raja Muda Abdul Aziz, Kuala Lumpur, Malaysia*
[b] *Tissue Engineering Centre, UKM Medical Centre, 56000, Cheras, Kuala Lumpur, Malaysia*

A B S T R A C T

A simple, cost-effective, and environmentally friendly method is needed for synthesizing metal nanoparticles, including gold nanoparticles (AuNPs). In this study, AuNPs were synthesized with *Lignosus rhinocerotis* sclerotial extract (LRE) and chitosan (CS) as reducing and stabilizing agents, respectively. Different LRE concentrations from cold and hot water extraction (CWE and HWE, respectively) were used to reduce chloroauric acid (HAuCl₄) to form AuNPs. Positively charged chitosan stabilized AuNPs (CS-AuNPs) mediated by LRE exhibited a surface plasmon resonance (SPR) band at 533 nm. The CS-AuNPs synthesized using CWE had a smaller particle size (49.5 ± 6.7–82.4 ± 28.0 nm) compared to that of the HWE samples (80.3 ± 23.4–125.3 ± 41.5 nm), depending on LRE concentration. FTIR results suggested protein and polysaccharides in LRE were the sources of reducing power, reducing gold ions to AuNPs. CS-AuNPs were mostly spherical with higher LRE concentrations, whereas some triangular, pentagonal, irregular, and rod shaped AuNPs were observed at lower LRE concentrations. CS-AuNPs mediated by LRE displayed effective antibacterial activity against gram-negative (*Pseudomonas aeruginosa* and *Escherichia coli*) and gram-positive bacteria (*Staphylococcus aureus* and *Bacillus* sp.). Thus, the biosynthesized AuNPs using LRE and chitosan provide opportunities for developing stable and eco-friendly nanoparticles with effective antibacterial properties.

1. Introduction

Pathogenic bacteria are microorganisms that cause infectious disease and can spread directly or indirectly between people via animal and insect vectors or from consumption of contaminated water, food, and other environmental exposures (Bethesda, 2007). Recently, gram-negative bacteria, such as *Pseudomonas aeruginosa* (*P. aeruginosa*) and gram-positive bacteria, such as *Staphylococcus aureus* (*S. aureus*) have developed increasing resistance towards conventional antibiotics (Frieria et al., 2017). Hence, the

development of effective antibacterial agents is urgently needed to treat antibiotic-resistant infections.

Nanoparticles refer to materials with particle sizes less than 100 nm (Mody et al., 2010). The large surface to volume ratio of nanoparticles due to their small particle size allows for the incorporation of many functional ligands which can enhance interactions with target bacteria (Li et al., 2014). Moreover, antibacterial activity of metal nanoparticles is affected by particle size and surface charge (Martinez-Castanon et al., 2008).

Recently, silver nanoparticles (AgNPs) and gold nanoparticles (AuNPs) have attracted significant interest due to their promising applications in the development of novel antibacterial agents. However, toxic effects and instability of AgNPs were reported previously (Ahamed et al., 2008; Nair and Laurencin, 2007). The toxicity of AgNPs was recently associated with their penetration and accumulation in the mitochondrial membrane that resulted in the impairment of mitochondrial function (Akter et al., 2018). Unlike AgNPs, AuNPs are more stable, inert, non-toxic and size-controllable. Moreover, Cui et al. (2012) reported that the antibacterial action of AuNPs did not trigger reactive oxygen species (ROS) generation, which may prevent harmful side-effects in mammalian host cells. AuNPs have also attracted more interest due to their

intense surface plasmon resonance (SPR) effect, originating from the interaction between an electromagnetic wave and electron conduction in metals (Bankar et al., 2010; Hu et al., 2006).

In conventional chemical syntheses of AuNPs, the reducing and stabilizing agents used are toxic and may cause adverse effects if they are adsorbed on the nanoparticles surface or accumulate in the environment (Dubey et al., 2010a,b; Noruzi et al., 2011). Currently, green synthesis or biosynthesis of AuNPs uses materials from natural sources, including plants extracts. For examples, *Alchemilla mollis* extract (Du et al., 2018), *Justicia glauca* leaf extract (Emmanuel et al., 2017) and *Punica granatum* peel extract (Kaviya, 2017). Other natural sources that have been recently applied to synthesize AuNPs include marine origin such as *Sargassum swartzii* (Dhas et al., 2016) and *Stephanopyxis turris* (Pytlik et al., 2017) as well as fungus (Narayanan et al., 2015). The green synthesis has garnered significant attention as a simple, rapid, cost effective, non-toxic, and environmentally benign method (Mohanpuria et al., 2008; Singh et al., 2013; Du et al., 2018).

Lignosus rhinocerotis (*L. rhinocerotis*), also known as Tiger milk mushroom, is a medicinal mushroom found in the tropical forests of Malaysia, Thailand, Indonesia, and China. The sclerotium of *L. rhinocerotis* is the part of the mushroom with medicinal properties. Traditionally, *L. rhinocerotis* has been used to relieve asthma, fever, and cough as well as to treat cancer, food poisoning, and wounds (Lee et al., 2009). More recently, *L. rhinocerotis* sclerotial extracts (LRE) has shown to exhibit anti-inflammatory (Lee et al., 2014), anti-proliferative (Lee et al., 2012) and antimicrobial activities (Mohanarji et al., 2012). Mushroom extracts contain constituents like terpenoids, tannins, polysaccharides, carbohydrates, phenolic compounds and flavonoids that could potentially act as reducing agents in biosynthesis of metal nanoparticles (Eskandari-Nojedehi et al., 2017). Metal nanoparticles tend to aggregate, grow into larger clusters, and eventually precipitate (Hettiarachchi and Wickramarachchi, 2011). Thus, a non-toxic, non-immunogenic, biocompatible, and degradable stabilizer is required in the production of AuNPs (Bonardda et al., 2016). Previously, chitosan (Sun et al., 2017) and its derivatives (Nazirov et al., 2016) have been used as a reducing and stabilizing agent for AuNPs synthesis. In this study, chitosan was used to stabilize LRE mediated AuNPs due to its ability to stabilize bare AuNPs (Esumi et al., 2003). The positively charged chitosan is vital in facilitating interactions with bacteria and has been credited with inherent antibacterial activity (Sarwar et al., 2015). The positively charged AuNPs can interact with the anionic cell membrane of gram-positive and -negative bacteria, resulting in the aggregation of AuNPs on the bacterial cell membrane and lysis of the bacterial cell (Hayden et al., 2012). In addition, blabbing caused by positively charged AuNPs disrupts the negatively charged bacterial cell membrane, leading to leakage of DNA from the damaged cell membrane (Zhao et al., 2010). In addition, chitosan has the potential to enhance biocompatibility of AuNPs.

In this study, biosynthesized AuNPs were produced using the combination of LRE and chitosan, which enables simultaneous synthesis and stabilization of AuNPs in a single pot. Although the antimicrobial activity of chitosan against bacteria and fungi has been explored well, however, this work explored the antibacterial activity of chitosan stabilized gold nanoparticles (CS-AuNPs) for the first time using LRE obtained by hot and cold water extraction (HWE and CWE, respectively). Besides, this study will facilitate exploration of medicinal benefits of LRE, laying a ground for the therapeutic use of *L. rhinocerotis.* CS-AuNPs were also characterized with respect to their SPR band, particle size, zeta potential, morphology, crystallinity, and antibacterial activity against selected gram-positive and negative bacteria.

2. Materials and methods

2.1. Materials

L. rhinocerotis sclerotial powder was provided as a gift from Lignas Bio Synergy, Selangor, Malaysia. Gold (III) chloride hydrate (99.999% trace metals basis) was procured from Sigma-Aldrich (Malaysia). Low molecular weight (LMW) chitosan (molecular weight of 190 kDa, 75–85% degree of deacetylation) was purchased from Sigma-Aldrich (Ireland). Glacial acetic acid (99.7% purity) was purchased from R&M Chemicals, UK. Distilled water was produced in the laboratory using a Hamilton WCS/85 cabinet water still. For antibacterial tests, four bacterial strains (*S. aureus*, *P. aeruginosa*, *Bacillus* sp., and *E. coli*) were obtained from Microbiologic Laboratory of the Faculty of Pharmacy, Universiti Kebangsaan Malaysia (Kuala Lumpur, Malaysia). Mueller-Hinton broth (MHB) and Mueller-Hinton agar (MHA) were purchased from Merck, Germany. Phosphate buffer saline (PBS) tablets were purchased from Invitrogen, USA. Gentamicin sulfate was purchased from Nacalai Tesque, Japan. All reagents were of analytical grade.

2.2. Methods

2.2.1. Preparation and phytochemical analysis of the cold water (CLRE) and hot water (HLRE) L. Rhinocerotis extracts

L. rhinocerotis sclerotial powder (100 g) was soaked in 2 L of distilled water at a ratio of 1:20 (w/v). The mixture was stirred continuously for 8 h at ambient temperature. After stirring, the mixture was filtered using Whatman No.1 filter paper, followed by centrifuging at 8000g (3700 revolutions per minute (rpm)) for 30 min (25 °C) using an Allegra 64R benchtop centrifuge (Beckman Coulter, Brea, California, USA). The supernatant was collected and filtered using Whatman No. 1 filter paper to remove insoluble materials. Extracts were stored in the refrigerator at 5 °C before use as a reducing agent. The same method was used to prepare the HLRE except the mixture was stirred continuously for 60 min at 90 °C after soaking the *L. rhinocerotis* sclerotial powder in 2 L of distilled water.

The phytochemical constituent analysis of LRE was carried out by liquid chromatography-mass spectrometry (LC-MS) analysis (Perkin Elmer Flexar FX15 UHPLC system coupled to Sciex 3200 hybrid trap triple quad tandem mass spectrometer) (UHPLC-MSMS (Model https://doi.org//1031491/K), Waltham, Massachusetts, USA). The extracts were diluted with 5 mL of distilled water prior to centrifugation at 8000 rpm for 3 min. The extracts were filtered through (0.45 μm Nylon syringe filter) prior to analysis using LC-MS.

The separation was achieved using a Phenomenex Synergy RP C18, 100 Å, 100 mm × 3 μm × 2.0 mm column. The run time was about 15 min with a back pressure of approximately 18,000 psi. The mobile phases comprised of (A) 0.1% formic acid in deionized water and (B) 0.1% formic acid in acetonitrile. The injection volume was 20 μL.

The MS conditions were set as follows: the scan was carried out in the mass range of 100–1200 m/z, at the source voltage of −4.5 kV and the source temperature of 500 °C in negative ionization mode. For MS/MS, the collision energy, collision energy spread and declustering potential was −35, 15, −60 V, respectively. The eluent was split and approximately 0.8 mL/min was introduced into the mass detector. Analyst® TF 1.5.2 software (Sciex) was used for data acquisition and analysis.

2.2.2. Biosynthesis of CS-AuNPs

Approximately 0.0225 g of LMW CS was dissolved in 6 mL of 2% v/v acetic acid under magnetic stirring at 500 rpm for 30 min.

Subsequently, 100 μL of 0.1 M $HAuCl_4$ solution was added to chitosan and different concentrations of CLRE solution (8 mL of 0.0125, 0.025, or 0.05 g/mL). The mixtures were continuously stirred under magnetic stirring and heating at 65 °C and pH 4.5 for 2.5 h until a stable purplish-wine color was observed. The resultant mixtures were cooled to room temperature and stored in the refrigerator at 5 °C for further studies. These steps were repeated for different concentrations of HLRE (0.0125, 0.025, and 0.05 g/mL).

2.2.3. UV–vis spectrophotometric

The formation of AuNPs was determined using a UV–vis Shimadzu 1800 spectrophotometer (High resolution (1 nm bandwidth), Shimadzu, Kyoto, Japan) by scanning the samples from 300 to 700 nm at a scan speed of 480 mm/min. Baseline correction of the spectrophotometer was performed using a blank reference.

2.2.4. ATR-FTIR spectroscopic analysis

Samples for Fourier transform infrared spectroscopy-attenuated total reflectance (FTIR-ATR) were prepared by freeze drying the LRE and resulting biosynthesized AuNPs modified with LRE and chitosan. The FTIR-ATR spectra of samples were recorded on a FTIR spectrometer (Spectrum 100; PerkinElmer, Walthman, MA, USA). The spectra were acquired using 32 scans and a 4 cm^{-1} resolution from 4000 to 650 cm^{-1}.

2.2.5. Particle size, polydispersity index (PDI), and zeta potential

The mean particle size (Z-average) as well as polydispersity index (PDI) and zeta potential (surface charge) of the freshly prepared biosynthesized AuNPs were measured by photon correlation spectroscopy (PCS, measurement range of 0.3–10 μm) and electrophoretic light scattering (measurement range of 3.8–100 μm), respectively using a ZS-90 Zetasizer (Malvern Instruments, Worcestershire, UK). All measurements were performed at 25 °C at a detection angle of 90°. Each sample was measured in triplicate and the data were reported as mean ± standard deviation (SD).

2.2.6. X-ray diffraction analysis

X-ray diffraction was used to characterize the structure of the crystalline CS-AuNPs. Samples were measured using a D8 Advance X-ray diffractometer (Bruker AXS GmbH, Karlsruhe, Germany) equipped with a high-speed energy-dispersive LYNXEYE XE-T detector.

2.2.7. Morphological analysis

Morphological characterization of the biosynthesized CS-AuNPs was performed using a transmission electron microscope (TEM) (Tecnai Spiri, FEI, Eindhoven, The Netherlands) with the resolution limit of about 0.2 nm. Samples for TEM analysis were prepared by placing drops of the CS-AuNP dispersions on carbon-coated TEM copper grids. The mixtures were allowed to evaporate at room temperature (25 ± 2 °C) for 1 min, and the extra solution was removed using blotting paper prior to viewing under the microscope.

2.2.8. Antibacterial tests

The antibacterial tests were performed using the agar well diffusion method (Rajan et al., 2017) with selected gram-positive (*S. aureus, P. aeruginosa*) and gram-negative bacteria (*Bacillus* sp. and *E. coli*). The bacterial strains were maintained in broth and subcultured in a petri dish prior to testing. First, 100 μL of CS-AuNPs was loaded into each hole on the Mueller Hinton (MH) agar plates and 100 μL of gentamicin (0.1 mg/mL) was loaded in the central hole as a positive control. The plates were subsequently sealed and incubated face upwards in an incubator (Memmert, Buchenbach, Germany) at 37 ± 0.2 °C for 24 h. The diameter of the inhibition zone (mm) was measured using an electronic digital Vernier caliper and was performed in triplicate.

2.2.9. Statistical analysis

All data were presented as the mean ± SD. The data were further analyzed using a two-way ANOVA, followed by post-hoc Tukey's or Bonferroni's test using GraphPad Prism software. Values of $p < 0.05$ indicated statistical significance among the groups tested.

3. Results and discussion

3.1. Formation of CS-AuNPs

The phytochemical analysis of CLRE and HLRE using LC-MS revealed that both contain oligosaccharides, polysaccharides, fatty acids and phenols (Fig. 1). These constituents could potentially act as reducing agents in the biosynthesis of AuNPs (Noruzi, 2015). The sclerotium of *L. rhinocerotis* was also reported to be rich in carbohydrates (Yap et al., 2015). The first observable indication for the formation of CS-AuNPs was a series of color changes in the reaction mixture, from pale yellow to light pink, pink, red wine, and finally to a purplish wine color (Fig. 2(A)). The color change could be firstly detected after 20 min. The color changed from colorless to wine purple indicated the formation of stabilized colloidal AuNPs (Simeonova et al., 2018). The color of the CS-AuNPs is attributed to SPR as a result of the collective oscillation of conduction band electrons induced by interacting electromagnetic fields (Philip et al., 2011). UV–vis spectroscopy is an indirect method to examine the bio-reduction of AuNPs from aqueous $HAuCl_4$ solution.

In this study, different concentrations (0.0125, 0.025, and 0.05 g/mL) of LRE influenced the formation of AuNPs. The UV–vis spectrum of the AuNPs showed an increase in peak intensity with increasing LRE concentration, indicating an increased number of AuNPs. This can be explained by the increased availability of reducing biomolecules in the LRE that are responsible for the reduction of gold ions at higher concentrations (Huang et al., 2007; Iravani, 2011; Sathishkumar et al., 2009). The absorbance peaks of the CS-AuNPs synthesized with CLRE (Fig. 2(B)(a)–(c)) are more intense than those synthesized using HLRE (Fig. 2(B)(d)–(f)). This is likely due to a larger amount of reducing biomolecules contained in the CLRE compared to the HLRE. The absorption bands of the AuNPs were observed at 533 nm, which is typical of the SPR band for AuNPs, demonstrating their successful formation. Likewise, visual inspection of the AuNP solution showed color changes from dark purple to a purplish-wine color with increasing LRE concentration.

3.2. Particle size, PDI, and zeta potential

Extracellular biosynthesis of AuNPs using plant extracts can be performed in a controlled manner, by tuning their size, shape, and dispersity (Kumar and Yadav, 2009). The particle size of AuNPs is influenced by the quantity of plant extract used, concentration of metal ions, reaction temperature, time, and pH (Iravani, 2011; Dubey et al., 2010a,b; Philip, 2009). In this study, the size of the AuNPs was investigated by varying the concentration of LRE and extraction method (CWE or HWE) used.

The CS-AuNPs increased in size with increasing LRE concentration, regardless of the type of extraction (CWE or HWE, Table 1). These results differed from those reported previously (Iravani, 2011; Song et al., 2009) that showed the opposite relationship. The CS-AuNPs synthesized using the CLRE were smaller in size (82.4 ± 28.0, 62.9 ± 5.8, and 49.5 ± 6.7 nm for 0.05, 0.025, and 0.0125 g/mL, respectively) than those synthesized using the HLRE (125.3 ± 41.5, 104.4 ± 11.2, and 80.3 ± 23.4 nm for 0.05, 0.025,
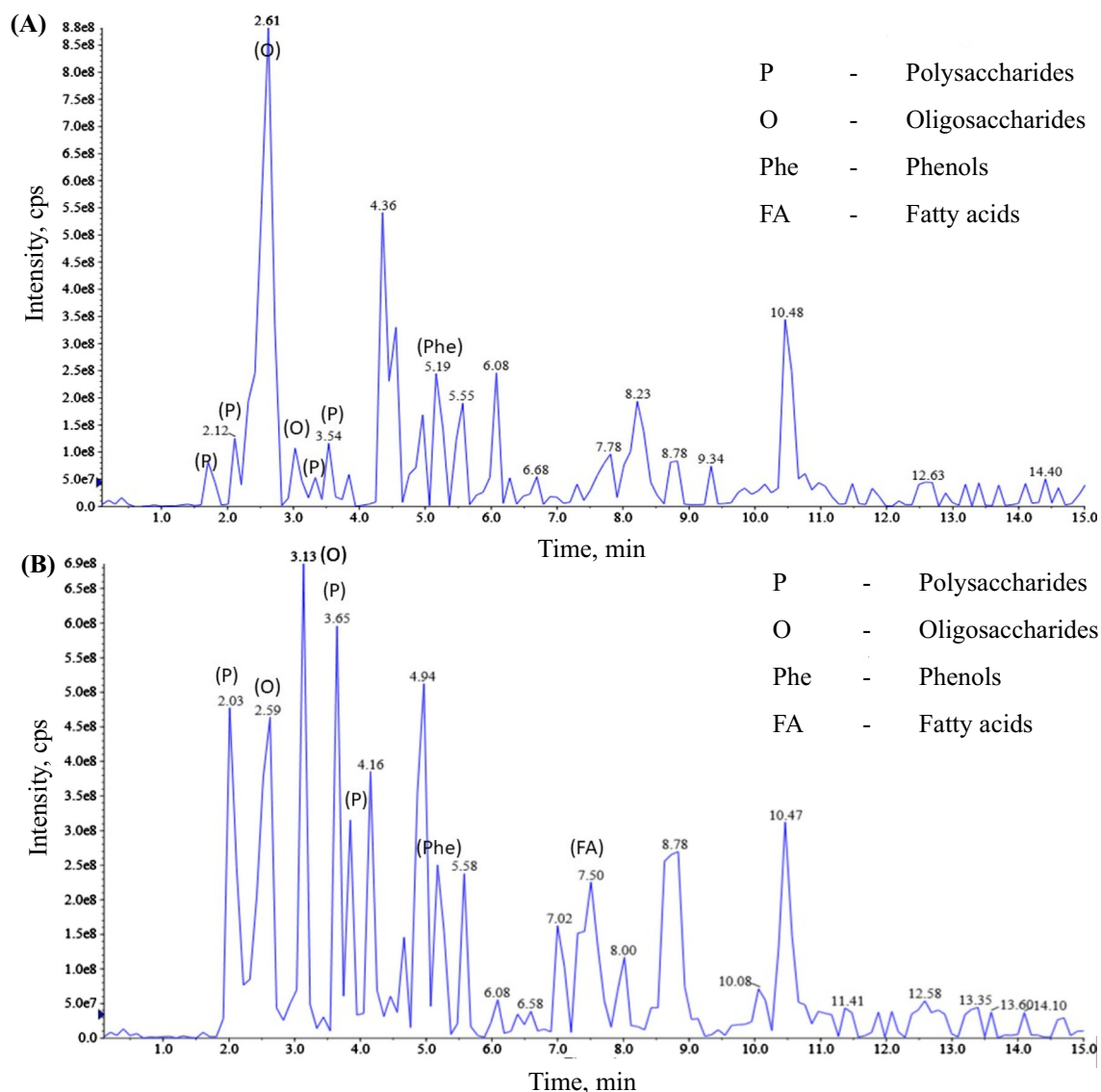
Fig. 1. Liquid chromatography-mass spectrometry (LC-MS) analysis of constituents in CLRE (A) and HLRE (B).

and 0.0125 g/mL, respectively). However, the size of the CS-AuNPs was not significantly affected by LRE concentrations (ANOVA, post-hoc analysis, $p > 0.05$ (Table Supplementary 2(a) and (b))). The PDI values of the CS-AuNPs were slightly above 0.5, except for that of the CS-AuNPs prepared using the CLRE at 0.0125 g/mL which had a lower value (Table 1) and was within the acceptable range.

As can be seen in Table 1, the zeta potential values of the CS-AuNPs were above +30 mV, except for those synthesized using the CLRE at 0.125 and 0.025 g/mL. The positive surface charge of AuNPs was attributed by protonation of chitosan's amino groups ($-NH_3^+$) in acidic condition (Simeonova et al., 2018). They were considered to be stable nanoparticles and were not prone to aggregation. Generally, AuNPs biosynthesized using plant extracts carry a negative charge on the particle surface (Koperuncholan, 2015). In this study, the biosynthesized CS-AuNPs carried a positive surface charge due to the presence of chitosan molecules (Esumi et al., 2003; Bhumkar et al., 2007). The electrostatic interaction between the positively charged amino groups in chitosan and AuNPs in solution effectively stabilized the nanoparticles (Huang and Yang, 2004) and later facil-itated interaction with the negatively charged bacterial cell wall.

On the other hand, the CS-AuNPs synthesized without the addi-tion of the LRE exhibited a larger particle size (151.7 ± 17.1 nm)

than those prepared with chitosan and LRE (Table 2). This could be explained by the influence of single and combinatory reducing agents on the size of the AuNPs as reported elsewhere (Alshammari et al., 2012). The combination of reductants can yield smaller AuNPs as compared to the use of either reductant in isola-tion. The combined action of LRE and chitosan in the synthesis of AuNPs was attributed to the generation of smaller particle size due to the synergistic stabilizing effect (Kim et al., 2016). This was further supported by the larger size of the AuNPs synthesized using LRE only which was beyond the desired range (data not included).

3.3. ATR-FTIR spectroscopic analysis

An infrared spectrum typically shows absorption bands relating to the bending or stretching of unique bonds and can be thought of as a sample fingerprint. A comparison of the ATR-FTIR spectra of chitosan, LRE, and the biosynthesized AuNPs is shown in Fig. 3 to provide further confirmation of successful CS-AuNPs formation. The spectrum of the LMW CS shows characteristic peaks at 3301.08 (−OH stretching), 2881.75 (−CH stretching), 1643.69 (−NH bending), and 1071.22 cm^{-1} (C−O−C stretching). These
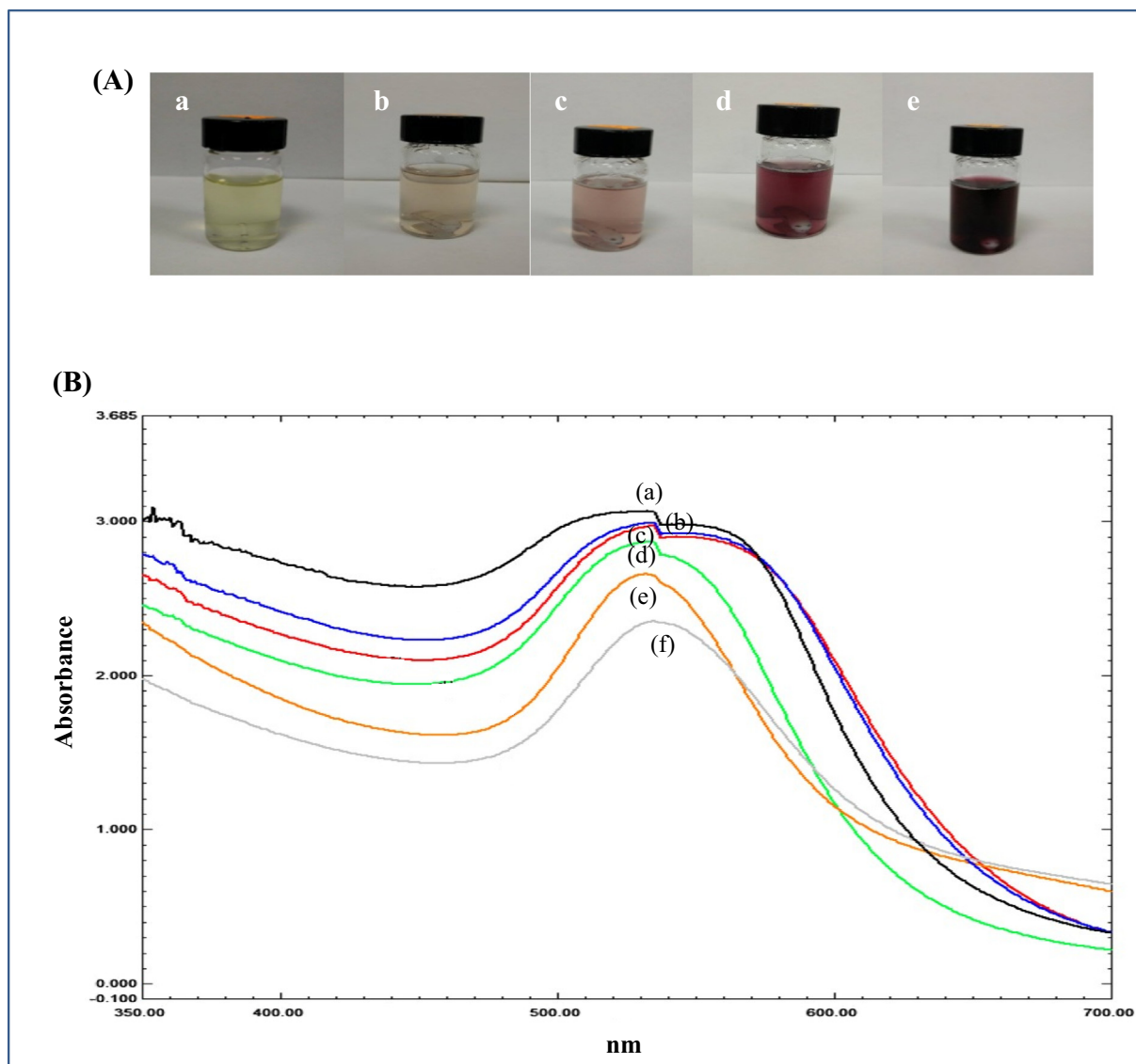
Fig. 2. (A) Color changes of in the reaction mixture at different time points: (a) pale yellow (0 min), (b) light pink (20 min), (c) pink (40 min), (d) red wine (60 min) and (e) purplish-wine color (150 min). (B) UV–vis spectrum of the CS-AuNPs synthesized from different concentrations of LRE (g/mL); from CWE at (a) 0.05, (b) 0.025, (c) 0.0125 g/mL as well as HWE at (d) 0.05, (e) 0.025 and (f) 0.0125 g/mL.

Table 1
Mean particle size, PDI, and zeta potential of the CS-AuNPs prepared with different concentrations of LRE (g/mL) from CWE and HWE, n = 3.

	LRE concentration (g/mL)	Particle size (nm) ± SD	PDI ± SD	Zeta potential (mV) ± SD
CWE	0.05	82.4 ± 28.0	0.69 ± 0.11	+30.8 ± 2.8
	0.025	62.9 ± 5.8	0.53 ± 0.22	+25.3 ± 4.0
	0.0125	49.5 ± 6.7	0.44 ± 0.02	+20.8 ± 5.5
HWE	0.05	125.3 ± 41.5	0.57 ± 0.04	+36.7 ± 1.4
	0.025	104.4 ± 11.2	0.57 ± 0.03	+38.7 ± 3.11
	0.0125	80.3 ± 23.4	0.52 ± 0.03	+38.8 ± 5.0

findings were similar to those reported elsewhere (Gregorio-Jauregui et al., 2012). In Fig. 3(a) and (b), the small bands at 1024.24 and 1025.61 cm^{-1} corresponded to the glucopyranose rings of chitosan, indicating attachment of chitosan to the AuNPs (Alkhatib et al., 2010) and suggesting the role of chitosan in stabilization of AuNPs. In acidic condition, amino groups of chitosan protonated and coated on the surface of AuNPs via electrostatic interaction, thus controlling the particle size and preventing aggregates formation due to repulsive force between particles, resulting in the well-stabilized nanoparticles (Le et al., 2014; Simeonova et al., 2018).

The major bioactive components of *L. rhinocerotis* sclerotial aqueous extract are polysaccharides, proteins, and polysaccharide-protein complexes (Lai et al., 2008). In this study, polysaccharides and oligosaccharides were the main constituents found in the LRE as determined by LC-MS analysis. The spectra of the CLRE (Fig. 3(a)) and HLRE (Fig. 3(b)) show IR band characteristic of hydroxyl groups (3280.41 and 3279.71 cm^{-1}), alkanes

Table 2
Zone of inhibition (mm) of *S. aureus*, *Bacillus* sp., *P. aeruginosa*, and *E. coli* for the CS-AuNPs prepared using different concentrations of LRE (g/mL) from CWE and HWE as well as gentamicin as a positive control, n = 3.

	LRE concentration (g/mL)	Zone of inhibition (mm)			
		S. aureus	*Bacillus* sp.	*P. aeruginosa*	*E. coli*
CWE	0.05	12.9 ± 0.3	–	15.2 ± 0.8	15.3 ± 0.7
	0.025	12.0 ± 0.4	–	16.0 ± 0.4	12.3 ± 0.3
	0.0125	11.4 ± 0.3	11.1 ± 0.1	15.4 ± 0.1	14.7 ± 0.4
HWE	0.05	10.7 ± 0.4	–	12.3 ± 0.5	12.6 ± 0.0
	0.025	11.2 ± 0.0	–	13.0 ± 0.5	12.3 ± 0.4
	0.0125	11.2 ± 0.59	–	14.0 ± 0.0	12.0 ± 0.4
Positive Control (Gentamicin)		22.3 ± 0.1	22.6 ± 0.1	20.3 ± 0.0	20.1 ± 0.5

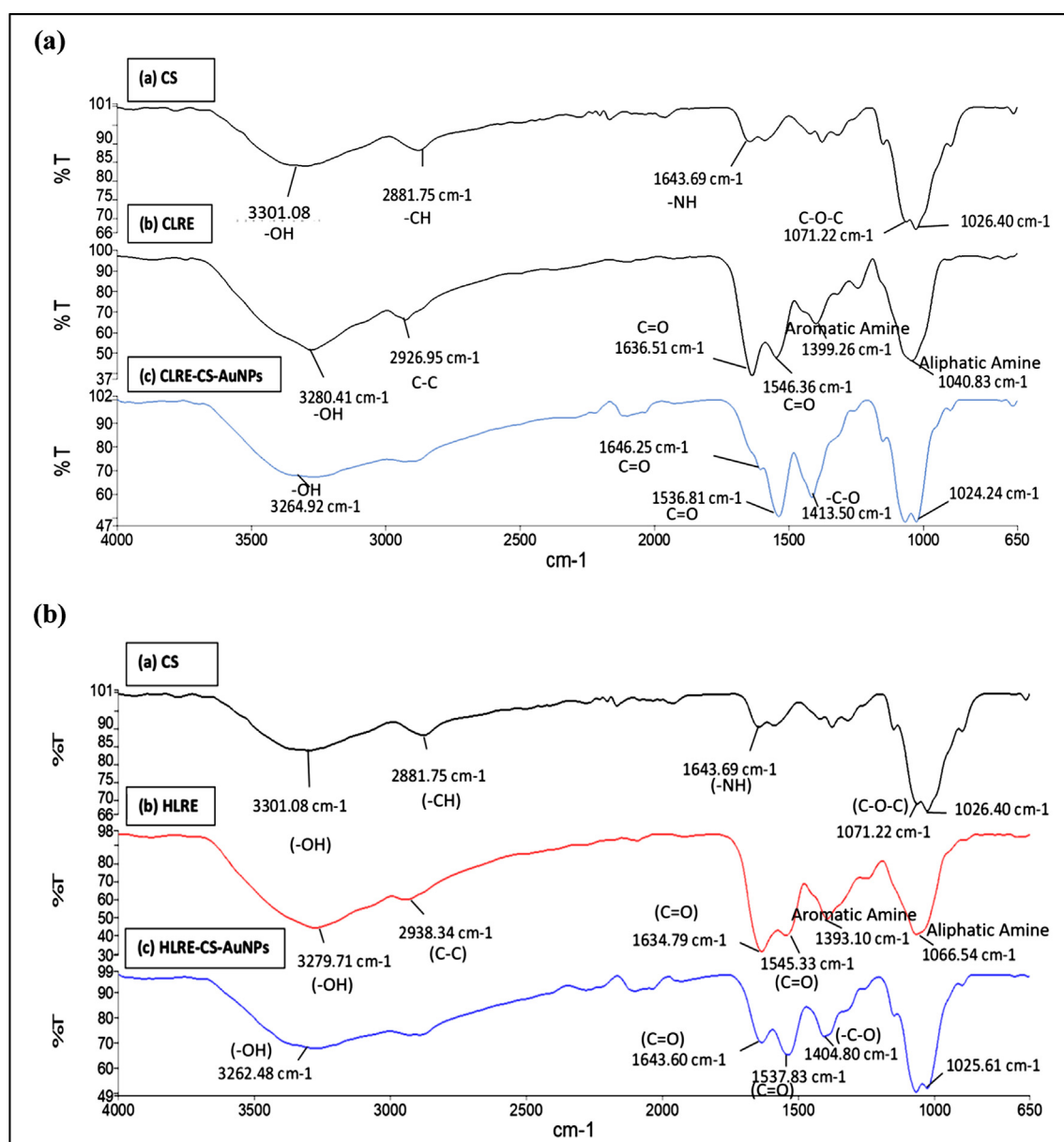Keynotes: "–" Zone of inhibition of bacteria unsubstantiated.

Fig. 3. FTIR spectra of (a) CS-AuNPs synthesized using CLRE with chitosan and CLRE only and (b) CS-AuNPs synthesized using HLRE with chitosan and HLRE only.

(2926.95 and 2938.34 cm^{-1}), amide I and II bands (1636.51 and 1546.36 cm^{-1}, 1634.79 and 1545.33 cm^{-1}, respectively) arising from proteins, aromatic amines (1399.26 and 1393.10 cm^{-1}), and aliphatic amines (1040.83 and 1066.54 cm^{-1}) (Das et al., 2011; Philip, 2010). In addition, the characteristic peaks corresponding to C—O—C vibrations of carbohydrate of polysaccharides appear at 1040.83 and 1066.54 cm^{-1} (Rajan et al., 2014) for CLRE and HLRE, respectively.

The spectra of the AuNPs synthesized from chitosan and LRE show broad intense peaks at $3264.92\ cm^{-1}$ (Fig. 3(a)) and $3262.48\ cm^{-1}$ (Fig. 3(b)), indicating that hydrogen bonding was enhanced between the —OH groups of LRE ($3280.41\ cm^{-1}$, Fig. 3 (a) or $3279.71\ cm^{-1}$, Fig. 3(b)) and chitosan ($3301.08\ cm^{-1}$) (Katas et al., 2012). In the LRE, hydroxyl groups (—OH) at 3200–$3600\ cm^{-1}$ from protein, polysaccharides and olisaccharides were involved in the formation of AuNPs by reducing Au(III) to Au(0) through oxidation of the hydroxyl group to form a carbonyl. This could be seen from the shift of characteristic peak corresponding to hydroxyl group from 3280.41 and $3279.71\ cm^{-1}$ for CLRE and HLRE, respectively to 3264.92 and $3262.48\ cm^{-1}$ for their resultant AuNPs. In biosynthesis of AuNPs, hydroxyl group plays a major role in the reduction of Au(III) to Au(0) (Mapala and Pattabi, 2017). This bio-reduction mechanism was also observed for biosynthesized AuNPs using brown algae, indicating the involvement of protein (Govindaraju et al., 2008) and polysaccharides (Noruzi, 2015) as possible bio-reductants.

The two bands at 1646.25 and $1536.81\ cm^{-1}$ (Fig. 3(a)) as well as 1643.60 and $1537.83\ cm^{-1}$ (Fig. 3(b)) were identified as amide I and II arising from the carbonyl stretch and —N—H stretch vibrations of the amide linkages in proteins. This suggests that the carbonyl groups in proteins, peptides, and amino acids of the LRE exhibit a strong ability to bind and react with gold (Vinod et al., 2011). The bands at 1413.50 and $1404.80\ cm^{-1}$ in the CS-AuNPs spectrum can be attributed to the —C—O stretching mode (Shankar et al., 2004). The spectra of the CS-AuNPs also indicate the successful formation of AuNPs as a result of the interaction between the LRE, chitosan and gold ions. Typical IR bands of LRE were observed in the AuNPs spectrum, suggesting strong interactions with the LRE during AuNP synthesis. The presence of different functional groups indicates the capping of biomolecules on the surface of AuNPs (Rajan et al., 2017). The proposed mechanism of surface coating of AuNPs by chitosan is shown in Fig. 4.

3.4. Morphology of the CS-AuNPs

The CS-AuNPs were mostly spherical in shape except for some that showed irregular, triangular, pentagonal, and rod shape nanoparticles particularly, for the low concentration of LRE

(0.0125 g/mL) (Fig. 5). Low concentrations of plant extract were reported to interact with gold ions to produce triangular and other irregular shapes. However, the addition of higher concentrations of plant extract led to the production of spherical shaped AuNPs (Song et al., 2009). Different shapes of AuNPs have been reported to affect their antibacterial activity. AuNPs with flower-shaped particles were more effective in killing *S. aureus* compared to those with star-shape and spherical particles as their sharp edges or protrusions could potentially pierce and rupture the bacterial membrane more efficiently (Penders et al., 2017).

The size of the CS-AuNPs ranged from 10 to 12 nm (10.6 ± 2.9, 11.9 ± 4.2, and 12.1 ± 4.1 nm for 0.05, 0.025, and 0.0125 g/mL, respectively) and 18 to 25 nm (17.7 ± 8.3, 18.9 ± 7.9, and 24.5 ± 6.4 nm for 0.05, 0.025, and 0.0125 g/mL, respectively) for the CLRE and HLRE preparations, respectively as determined by TEM. This matches the results obtained from photon correlation spectroscopy (PCS) which showed the size of the AuNPs prepared from HLRE was larger than that of the CLRE preparation. Despite that, the measured particle size using TEM was smaller than those obtained from PCS technique, possibly due to different sample condition. Generally, particle size measured from PCS is larger than TEM because PCS measures hydrodynamic sizes in which particles are suspended in liquid medium while dry samples are used in TEM analysis (He and Zhao, 2007; Simeonova et al., 2018). In Fig. 5(c), the CS-AuNPs formed using CLRE at 0.0125 g/mL were observed to aggregate to some extent due to their low zeta potential ($+20.8 \pm 5.5$ mV), indicating decreased stability of the colloidal system compared to the other preparations. The other CS-AuNPs were well dispersed in the colloidal solution and particle aggregation was not observed.

3.5. X-ray diffraction analysis

X-ray diffraction is an important technique for structural characterization of crystalline materials (Malarkodi et al., 2013). X-ray diffraction of the CS-AuNPs synthesized using the CLRE and HLRE are shown in Fig. 6 and the crystalline structure of both samples was confirmed. The CS-AuNPs synthesized using the CLRE match the gold standard published by JCPDS (file no. 04-0784, 71-4614 and 71-4616) while the AuNPs synthesized using the HLRE match
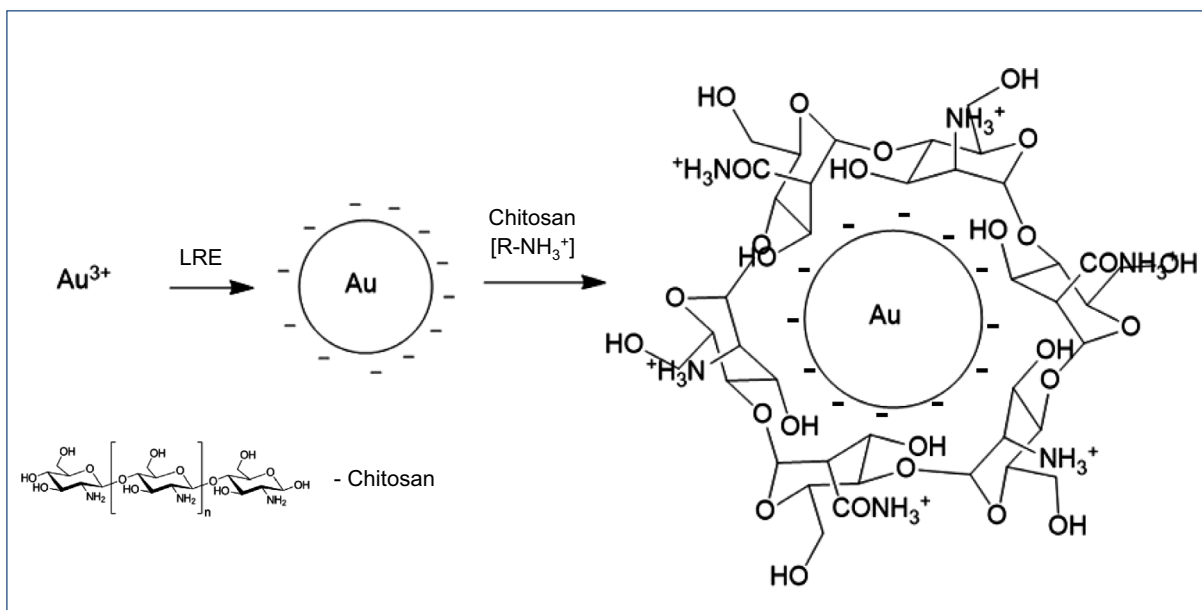

Fig. 4. Proposed mechanism of surface coating of AuNPs by chitosan. In the first step, LRE reduce tetrachloroauric acid into AuNPs and in the second step, AuNPs are coated with chitosan via electrostatic interactions between positively charged amino groups of chitosan and negatively charged AuNPs.
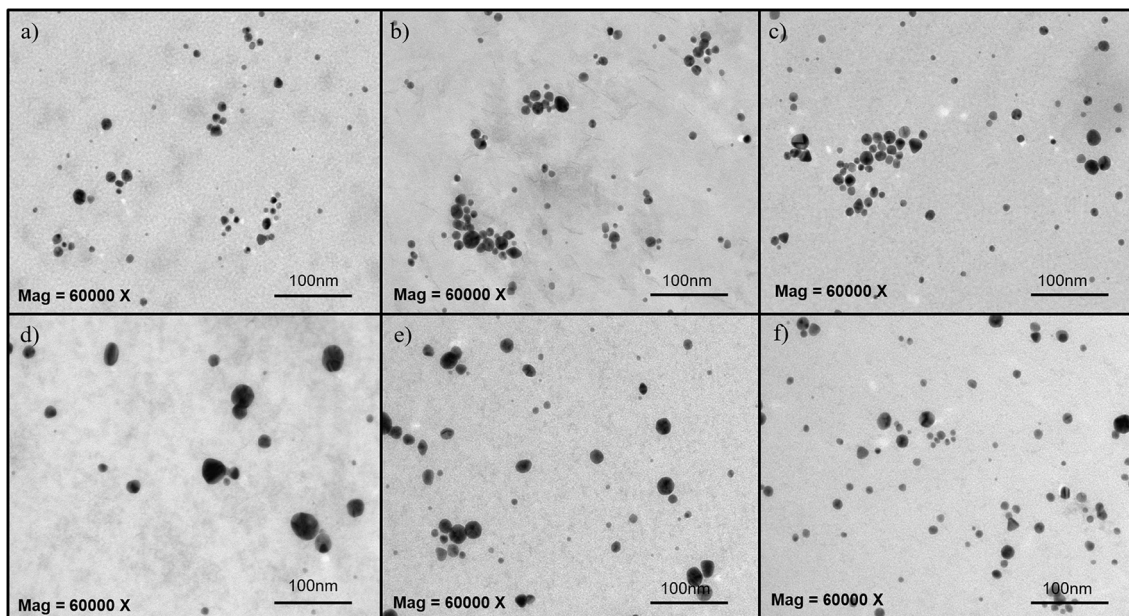
Fig. 5. TEM images of the CS-AuNPs prepared with different LRE concentrations from CWE at (a) 0.05, (b) 0.025, (c) 0.0125 g/mL as well as HWE at (d) 0.05, (e) 0.025 and (f) 0.0125 g/mL. The magnification of the images is 60,000×.
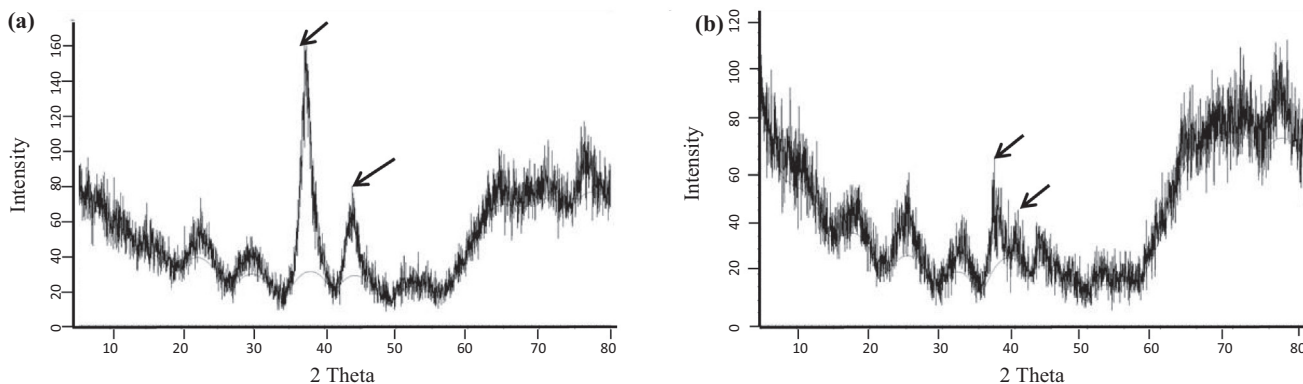

Fig. 6. X-ray diffraction of the CS-AuNPs synthesized using CLRE (a) and HLRE (b).

with JCPDS (file no. 65-8601, 71-4615 and 04-0784). In a study by Malarkodi et al. (2013), the X-ray diffraction (XRD) facets of AuNPs was also compared and matched with the gold standard of JCPDS (file no. 04-0784).

The percentage of crystallinity observed in the CS-AuNPs synthesized by CLRE was higher (33.1%) compared to those prepared with HLRE (23.95%). Their peak is also sharper, which clearly indicates improved crystallinity. The CS-AuNPs synthesized by CLRE and HLRE exhibited four prominent Bragg reflections at approximately 38.179, 44.379, 65.545, and 77.558° as well as 38.111, 44.243, 64.409, and 77.286°, respectively.

3.6. Antibacterial activity of the biosynthesized AuNPs

In this study, all bacteria tested were affected by the CS-AuNPs except for *Bacillus* sp., which was only affected by the AuNPs prepared using CLRE at 0.0125 g/mL. Their inhibition zones from agar-well diffusion assay are shown in Supplementary 1. From Table 3, it can be seen that the antibacterial activity of the CS-AuNPs was more effective against gram-negative bacteria compared to gram-positive bacteria although the LRE from CWE and HWE did not show any antibacterial activity as determined by

agar-well diffusion and broth microdilution methods. The findings were differ from a previous study by Mohanarji et al. (2012) that showed high antibacterial activity of the extracts against selected human pathogens, probably due to different extraction methods used in both studies. Different extracts may contain different phytochemical constituents with different pharmacological properties. The improved antibacterial activity against gram-negative bacteria can be attributed to the thinner cell wall of gram-negative bacteria,

Table 3
Zone of inhibition (mm) of *S. aureus* and *P. aeruginosa* for the AuNPs synthesized using chitosan only (absence of LRE), n = 3.

Chitosan concentration (g/mL)	Zone of Inhibition (mm)	
	S. aureus	*P. aeruginosa*
0.2	7.0 ± 6.3	3.8 ± 6.6
0.4	6.8 ± 6.1	6.9 ± 6.1
0.6	7.1 ± 6.3	9.9 ± 2.0
0.8	10.5 ± 2.6	9.9 ± 1.5
1.0	10.7 ± 2.3	9.9 ± 1.0
1.2	10.6 ± 1.8	10.3 ± 1.5
Positive Control (Gentamicin)	21.5 ± 8.7	21.5 ± 10.0

making them more susceptible to the action of the CS-AuNPs. Gram-positive bacteria have a cell wall with a thicker layer of peptidoglycan that can impede the uptake of AuNPs (Da Silva et al., 2010; No et al., 2002; Venkatpurwar and Pokharkar, 2011).

Furthermore, the CS-AuNPs synthesized using CLRE were more effective against bacteria than those prepared using HLRE. This can be attributed to the smaller particle size of the CS-AuNPs synthesized using CLRE which provide larger surface-to-volume ratio and more effective contact with the bacterial surface, enhancing antimicrobial efficiency (Ye et al., 2005). In addition, cationic chitosan exhibits antibacterial activity via its strong ionic interaction with bacteria (Ye et al., 2005). By adding the LRE, the resulting CS-AuNPs exhibited higher antibacterial activity against gram-positive bacteria, although these bacteria have a thicker peptidoglycan layer in their cell walls that is more resistance towards antibacterial agent compared to gram-negative bacteria. For gram-positive bacteria, a higher concentration of AuNPs may be required to inhibit growth (Venkatpurwar and Pokharkar, 2011). No distinct trend was observed in the antibacterial activity of CS-AuNPs prepared with different concentrations of LRE although the low concentration of LRE had more irregular, triangular and pentagonal shape particles. However, a significant difference in the antibacterial efficacy of CS-AuNPs synthesized using either HLRE or CLRE (ANOVA, Bonferroni's post hoc analysis, $p < 0.05$ (Table Supplementary 2 (c), (d), (e) and (f))) was observed for *P. aeruginosa*, *S. aureus*, and *E. coli*. This indicated that the extraction method significantly influenced the antibacterial activity, which might also be affected by the size of the CS-AuNPs. Both factors were identified to play a more prominent role in contributing to the antibacterial effect as compared to other factor like particle shape.

The antibacterial activity of CS-AuNPs synthesized without the addition of LRE was also tested against *S. aureus* and *P. aeruginosa*. AuNPs that are surrounded by stabilizer molecules such as chitosan do not agglomerate, show reduced surface area, and smaller interfacial free energy, allowing the reactivity of the particles to be maintained for long periods (Prema, 2013). In this experiment, the CS-AuNPs (without LRE extract treatment) were prepared with varying chitosan concentrations (0.2, 0.4, 0.6, 0.8, 1.0, and 1.2% w/v). Both bacteria *S. aureus* and *P. aeruginosa* were also affected by the CS-AuNPs. The zone of inhibition increased for both bacteria when the concentration of chitosan was increased and *S. aureus* was more affected by the AuNPs compared to *P. aeruginosa*. The largest zone of inhibition recorded for *S. aureus* was with the CS-AuNPs prepared with a chitosan concentration of 1% w/v, while the CS-AuNPs prepared with 1.2% w/v chitosan was most active towards *P. aeruginosa*. Previously, AuNPs have been shown to exhibit strong antibacterial activity towards *S. aureus* and *E. coli* (MubarakAli et al., 2011).

The concentration of chitosan needed to synthesize antibacterial CS-AuNPs with LRE was lower than those without LRE, suggesting that the addition of LRE as reducing agent resulted in higher antibacterial activity. Thus, chitosan as a stabilizing or capping agent and LRE as a reducing agent for the production of AuNPs improved antibacterial activity of their resultant nanoparticles.

4. Conclusions

Cationic CS-AuNPs formed using CLRE exhibited smaller particle sizes than those formed using HLRE. They were mostly spherical in shape and exhibited higher antibacterial activity than those synthesized from HLRE. Moreover, the CS-AuNPs biosynthesized with LRE and chitosan show promise as antibacterial agents against bacteria, particularly gram-negative bacteria that may be resistant to traditional antibiotics.

Appendix A. Supplementary material

Supplementary data to this article can be found online at https://doi.org/10.1016/j.jsps.2018.11.010.

References

Ahamed, M., Karns, M., Goodson, M., Rowe, J., Hussain, S.M., Schlager, J.J., Hong, Y., 2008. DNA damage response to different surface chemistry of silver nanoparticles in mammalian cells. Toxicol. Appl. Pharmacol. 233, 404–410.

Akter, M., Sikder, M.T., Rahman, M.M., Ullah, A.K.A.M., Hossain, K.F.B., Banik, S., Hosokawa, T., Saito, T., Kurasaki, M., 2018. A systematic review on silver nanoparticles-induced cytotoxicity: Physicochemical properties and perspectives. J. Adv. Res. 9, 1–16.

Alkhatib, M.F., Mirghani, M.E.S., Qudsieh, I.Y., Husain, I.A., 2010. Immobilization of chitosan onto carbon nanotubes for lead removal from water. J. Appl. Sci. 10, 2705–2708.

Alshammari, A., Köckritz, A., Kalevaru, V.N., Bagabas, A., Martin, A., 2012. Influence of single use and combination of reductants on the size, morphology and growth steps of gold nanoparticles in colloidal mixture. Open J. Phys. Chem. 2, 252–261.

Bankar, A., Joshi, B., Kumar, A.R., Zinjarde, S., 2010. Banana peel extract mediated synthesis of gold nanoparticles. Colloids Surf. B 80, 45–50.

Bethesda (MD), 2007. Understanding emerging and re-emerging infectious diseases. In: National Institutes of Health Curriculum Supplement Series [Internet]. Biological Sciences Curriculum Study, National Institutes of Health (US). https://www.ncbi.nlm.nih.gov/books/NBK20370/ (accessed 13.03.03).

Bhumkar, D.R., Joshi, H.M., Sastry, M., Pokharkar, V.B., 2007. Chitosan reduced gold nanoparticles as novel carriers for transmucosal delivery of insulin. Pharm. Res. 24, 1415–1426.

Bonardda, S., Schmidta, M., Saavedra-Torres, M., Leivaa, A., Radica, D., Saldías, C., 2016. Thermal and morphological behavior of chitosan/PEO blends containing gold nanoparticles. Experimental and theoretical studies. Carbohydr. Polym. 130, 315–329.

Cui, Y., Zhao, Y., Tian, Y., Zhang, W., Lü, X., Jiang, X., 2012. The molecular mechanism of action of bactericidal gold nanoparticles on Escherichia coli. Biomater. 33, 2327–2333.

Dhas, T.S., Kumar, V.G., Karthick, V., Vasanth, K., Singaravelu, G., Govindaraju, K., 2016. Effect of biosynthesized gold nanoparticles by *Sargassum swartzii* in alloxan induced diabetic rats. Enzyme Microbiol. Technol. 95, 100–106.

Da Silva, L.P., De Britto, D., Seleghim, M.H.R., Assis, O.B., 2010. *In vitro* activity of water-soluble quaternary chitosan chloride salt against *E. Coli*. World J. Microbiol. Biotechnol. 26, 2089–2092.

Das, R.K., Gogoi, N., Bora, U., 2011. Green synthesis of gold nanoparticles using Nyctanthes arbortristis flower extract. Bioprocess. Biosyst. Eng. 34, 615–619.

Dubey, S.P., Lahtinen, M., Sillanpää, M., 2010a. Green synthesis and characterizations of silver and gold nanoparticles using leaf extract of Rosa rugosa. Colloids Surf. A 364, 34–41.

Dubey, S.P., Lahtinen, M., Sillanpää, M., 2010b. Tansy fruit mediated greener synthesis of silver and gold nanoparticles. Process Biochem. 45, 1065–1071.

Du, J., Singh, H., Dong, W.-J., Bai, Y.-H., Yi, T.-H., 2018. Colorimetric detection of *Listeria monocytogenes* using one-pot biosynthesized flower-shaped gold nanoparticles. Sens. Actuators B. Chem. 265, 285–292.

Emmanuel, R., Saravanan, M., Ovais, M., Padmavathy, S., Shinwari, Z.K., Prakash, P., 2017. Antimicrobial efficacy of drug blended biosynthesized colloidal gold nanoparticles from *Justicia glauca* against oral pathogens: a nanoantibiotic approach. Microbiol. Pathog. 113, 295–302.

Eskandari-Nojedehi, M., Jafarizadeh-Malmiri, H., Rahbar-Shahrouzi, J., 2017. Hydrothermal green synthesis of gold nanoparticles using mushroom (Agaricus bisporus) extract: physico-chemical characteristics and antifungal activity studies. Green Process Synth, aop: 1-10.

Esumi, K., Takei, N., Yoshimura, T., 2003. Antioxidant-potentiality of gold–chitosan nanocomposites. Colloids Surf. B 32, 117–123.

Frieria, M., Kumar, K., Boutin, A., 2017. Antibiotic resistance. J. Infect. Public Health 10, 369–378.

Govindaraju, K., Basha, S.K., Kumar, V.G., Singaravelu, G., 2008. Silver, gold and bimetallic nanoparticles production using single-cell protein (Spirulina platensis) Geitler. J. Mater. Sci. 43, 5115–5122.

Gregorio-Jauregui, K.M., Pineda, M.G., Rivera-Salinas, J.E., Hurtado, G., Saade, H., Martinez, J.L., Ilyina, A., López, R.G., 2012. One-step method for preparation of magnetic nanoparticles coated with chitosan. J. Nanomater.

Hayden, S.C., Zhao, G., Saha, K., Phillips, R.L., Li, X., Miranda, O.R., Rotello, V.M., El-Sayed, M.A., Schmidt-Krey, I., Bunz, U.H., 2012. Aggregation and interaction of cationic nanoparticles on bacterial surfaces. J. Am. Chem. Soc. 134, 6920–6923.

He, F., Zhao, D., 2007. Manipulating the size and dispersibility of zerovalent iron nanoparticles by use of carboxymethyl cellulose stabilizers. Environ. Sci. Technol. 41, 6216–6221.

Hettiarachchi, M., Wickramarachchi, P., 2011. Synthesis of chitosan stabilized silver nanoparticles using gamma ray irradiation and characterization. J. Sci. 6, 65–75.

Hu, M., Chen, J., Li, Z.-Y., Au, L., Hartland, G.V., Li, X., Marquez, M., Xia, Y., 2006. Gold nanostructures: engineering their plasmonic properties for biomedical applications. Chem. Soc. Rev. 35, 1084–1094.

Huang, H., Yang, X., 2004. Synthesis of chitosan-stabilized gold nanoparticles in the absence or presence of tripolyphosphate. Biomacromol. 5, 2340–2346.

Huang, J., Li, Q., Sun, D., Lu, Y., Su, Y., Yang, X., Wang, H., Wang, Y., Shao, W., He, N., 2007. Biosynthesis of silver and gold nanoparticles by novel sundried Cinnamomum camphora leaf. Nanotechnol. 18, 105104.

Iravani, S., 2011. Green synthesis of metal nanoparticles using plants. Green Chem. 13, 2638–2650.

Katas, H., Hussain, Z., Ling, T.C., 2012. Chitosan nanoparticles as a percutaneous drug delivery system for hydrocortisone. J. Nanomat. 1.

Kaviya, S., 2017. Rapid naked eye detection of arginine by pomegranate peel extract stabilized gold nanoparticles. J. King Saud Univ. – Sci. corrected proof (in press). https://doi.org/10.1016/j.jksus.2017.12.001.

Kim, H.-S., Seo, Y.S., Kim, K., Han, J.W., Park, Y., Cho, S., 2016. Concentration effect of reducing agents on green synthesis of gold nanoparticles: size, morphology, and growth mechanism. Nanoscale Res. Lett. 11, 230.

Koperuncholan, M., 2015. Bioreduction of chloroauric acid (HAuCl4) for the synthesis of gold nanoparticles (GNPs): a special empathies of pharmacological activity. Int. J. Phytopharm. 5, 72–80.

Kumar, V., Yadav, S.K., 2009. Plant-mediated synthesis of silver and gold nanoparticles and their applications. J. Chem. Technol. Biotechnol. 84, 151–157.

Lai, C.K., Wong, K.-H., Cheung, P.C.K., 2008. Antiproliferative effects of sclerotial polysaccharides from Polyporus rhinocerus Cooke (Aphyllophoromycetideae) on different kinds of leukemic cells. Int. J. Med. Mushrooms. 10, 255–264.

Le, T.L., Dinh, Q.K., Tran, T.H., Nguyen, H.P., Hoang, T.L.H., Nguyen, Q.H., 2014. Synthesis of water soluble chitosan stabilized gold nanoparticles and determination of uric acid. Adv. Nat. Sci: Nanosci. Nanotechnol. 5, 025014.

Lee, M.L., Tan, N.H., Fung, S.Y., Tan, C.S., Ng, S.T., 2012. The antiproliferative activity of sclerotia of Lignosus rhinocerus (Tiger milk mushroom), BMC Complement. Altern. Med. 5, 1–5.

Lee, S.S., Chang, Y.S., Noraswati, M.N.R., 2009. Utilization of macrofungi by some indigenous communities for food and medicine in peninsular Malaysia. Forest Ecol. Manage. 257, 2062–2065.

Lee, S.S., Tan, N.H., Fung, S.Y., Sim, S.M., Tan, C.S., Ng, S.T., 2014. Anti-inflammatory effect of the sclerotium of Lignosus rhinocerotis (Cooke) Ryvarden, the Tiger milk mushroom, BMC Complement. Altern. Med. 14, 1–8l.

Li, X., Robinson, S.M., Gupta, A., Saha, K., Jiang, Z., Moyano, D.F., Sahar, A., Riley, M.A., Rotello, V.M., 2014. Functional gold nanoparticles as potent antimicrobial agents against multi-drug-resistant bacteria. ACS Nano 8, 10682–10686.

Malarkodi, C., Rajeshkumar, S., Vanaja, M., Paulkumar, K., Gnanajobitha, G., Annadurai, G., 2013. Eco-friendly synthesis and characterization ofgold nanoparticles using Klebsiella pneumoniae. J. Nanostruct. Chem. 3, 1–7.

Mapala, K., Pattabi, M., 2017. Mimosa pudica flower extract mediated green synthesis of gold ganoparticles. NanoWorld J. 3, 44–50.

Martinez-Castanon, G., Nino-Martinez, N., Martinez-Gutierrez, F., Martinez-Mendoza, J., Ruiz, F., 2008. Synthesis and antibacterial activity of silver nanoparticles with different sizes. J. Nanopart. Res. 10, 1343–1348.

Mody, V.V., Siwale, R., Singh, A., Mody, H.R., 2010. Introduction to metallic nanoparticles. J. Pharm. Bioallied. Sci. 2, 282–289.

Mohanarji, S., Dharmalingam, S., Kalusalingam, A., 2012. Screening of Lignosus rhinocerus extracts as antimicrobial agents against selected human pathogens. J. Pharm. Biomed. Sci. 18, 1–4.

Mohanpuria, P., Rana, N.K., Yadav, S.K., 2008. Biosynthesis of nanoparticles: technological concepts and future applications. J. Nanopart. Res. 10, 507–517.

MubarakAli, D., Thajuddin, N., Jeganathan, K., Gunasekaran, M., 2011. Plant extract mediated synthesis of silver and gold nanoparticles and its. Colloids Surf. B Biointerfaces 85, 360–365.

Nair, L.S., Laurencin, C.T., 2007. Silver nanoparticles: synthesis and therapeutic applications. J. Biomed. Nanotechnol. 3, 301–316.

Narayanan, K.B., Park, H.H., Han, S.S., 2015. Synthesis and characterization of biomatrixed-gold nanoparticles by the mushroom Flammulina velutipes and its heterogeneous catalytic potential. Chemosphere 141, 169–175.

Nazirov, A., Pestov, A., Privar, Y., Ustinov, A., Modin, E., Bratskaya, S., 2016. One-pot green synthesis of luminescent gold nanoparticles using imidazole derivative of chitosan. Carbohydr. Polym. 20, 649–655.

No, H.K., Park, N.Y., Lee, S.H., Meyers, S.P., 2002. Antibacterial activity of chitosans and chitosan oligomers with different molecular weights. Int. J. Food Microbiol. 74, 65–72.

Noruzi, M., 2015. Biosynthesis of gold Nanoparticles using plant extracts. Bioprocess. Biosyst. Eng. 38, 1–14.

Noruzi, M., Zare, D., Khoshnevisan, K., Davoodi, D., 2011. Rapid green synthesis of gold nanoparticles using Rosa hybrida petal extract at room temperature. Spectrochim. Acta A 79, 1461–1465.

Penders, J., Stolzoff, M., Hickey, D.J., Andersson, M., Webster, T.J., 2017. Shape-dependent antibacterial effects of non-cytotoxic gold nanoparticles. Int. J. Nanomed. 29, 2457–2468.

Philip, D., 2009. Biosynthesis of Au, Ag and Au–Ag nanoparticles using edible mushroom extract. Spectrochim. Acta. A 73, 374–381.

Philip, D., 2010. Rapid green synthesis of spherical gold nanoparticles using Mangifera indica leaf. Spectrochim. Acta. A. 77, 807–810.

Philip, D., Unni, C., Aromal, S.A., Vidhu, V., 2011. Murraya koenigii leaf-assisted rapid green synthesis of silver and gold nanoparticles. Spectrochim. Acta. A. 78, 899–904.

Prema, P.T.S., 2013. In-vitro antibacterial activity of gold nanoparticles capped with polysaccharide stabilising agents. Int. J. Pharm. Pharm. Sci. 5, 310–314.

Pytlik, N., Kaden, J., Finger, M., Naumann, J., Brunner, E., 2017. Biological synthesis of gold nanoparticles by the diatom Stephanopyxis turris and in vivo SERS analyses. Algal Res. 28, 9–15.

Rajan, A., Kumari, M.M., Philip, D., 2014. Shape tailored green synthesis and catalytic properties of gold nanocrystals. Spectrochim. Acta A 118, 793–799.

Rajan, A., Rajan, A.R., Philip, D., 2017. Elettaria cardamomum seed mediated rapid synthesis of gold nanoparticles and its biological activities. OpenNano 2, 1–8.

Sarwar, A., Katas, H., Samsudin, S.N., Zin, N.M., 2015. Regioselective sequential modification of chitosan via azide-alkyne click reaction: synthesis, characterization, and antimicrobial activity of chitosan derivatives and nanoparticles. PLoS One 10, e0123084.

Sathishkumar, M., Sneha, K., Won, S., Cho, C.-W., Kim, S., Yun, Y.-S., 2009. Cinnamon zeylanicum bark extract and powder mediated green synthesis of nano-crystalline silver particles and its bactericidal activity. Colloids Surf. B 73, 332–338.

Simeonova, S., Georgiev, P., Exner, K.S., Mihaylov, L., Nihtianova, D., Koynov, K., Balashev, K., 2018. Kinetic study of gold nanoparticles synthesized in the presence of chitosan and citric acid. Colloids Surf. A 557, 106–115.

Shankar, S.S., Rai, A., Ahmad, A., Sastry, M., 2004. Rapid synthesis of Au, Ag, and bimetallic Au core–Ag shell nanoparticles using neem (Azadirachta indica) leaf broth. J. Colloid Interface Sci. 275, 496–502.

Singh, M., Kalaivani, R., Manikandan, S., Sangeetha, N., Kumaraguru, A., 2013. Facile green synthesis of variable metallic gold nanoparticle using Padina gymnospora, a brown marine macroalga. Appl. Nanosci. 3, 145–151.

Song, J.Y., Jang, H.-K., Kim, B.S., 2009. Biological synthesis of gold nanoparticles using Magnolia kobus and Diopyros kaki leaf extracts. Process Biochem. 44, 1133–1138.

Sun, L., Li, J., Cai, J., Zhong, L., Ren, G., Ma, Q., 2017. One pot synthesis of gold nanoparticles using chitosan with varying degree of deacetylation and molecular weight. Carbohydr. Polym. 178, 105–114.

Venkatpurwar, V., Pokharkar, V., 2011. Green synthesis of silver nanoparticles using marine polysaccharide: study of in-vitro antibacterial activity. Mater. Lett. 65, 999–1002.

Vinod, V., Saravanan, P., Sreedhar, B., Devi, D.K., Sashidhar, R., 2011. A facile synthesis and characterization of Ag, Au and Pt nanoparticles using a natural hydrocolloid gum kondagogu (Cochlospermum gossypium). Colloids Surf. B 83, 291–298.

Yap, H.Y., Fung, S.Y., Tan, C.S., Tan, N.H., 2015. genome-based proteomic analysis of lignosus rhinocerotis (cooke) ryvarden sclerotium. Int. J. Med. Sci 12, 23–31.

Ye, W., Leung, M.F., Xin, J., Kwong, T.L., Lee, D.K.L., Li, P., 2005. Novel core-shell particles with poly (N-butyl acrylate) cores and chitosan shells as an antibacterial coating for textiles. Polymer 46, 10538–10543.

Zhao, Y., Tian, Y., Cui, Y., Liu, W., Ma, W., Jiang, X., 2010. Small molecule-capped gold nanoparticles as potent antibacterial agents that target Gram-negative bacteria. J. Am. Chem. Soc. 132, 12349–12356.